ELSEVIER

Applied Surface Science 175–176 (2001) 428–435

applied surface science

www.elsevier.nl/locate/apsusc

The electrical properties of MIS capacitors with ALN gate dielectrics

T. Adam[a,*], J. Kolodzey[a], C.P. Swann[b], M.W. Tsao[c], J.F. Rabolt[c]

[a]*Department of Electrical and Computer Engineering, University of Delaware, Newark, DE 19716, USA*
[b]*Bartol Research Institute, University of Delaware, Newark, DE 19716, USA*
[c]*Department of Materials Science and Engineering, University of Delaware, Newark, DE 19716, USA*

Accepted 16 November 2000

Abstract

We report on the characteristics of metal–insulator–semiconductor (MIS) capacitors with aluminum nitride (AlN) as the dielectric material. Using reactive magnetron sputtering, we deposited layers of AlN on 1–10 Ω cm p-type (1 0 0) silicon wafers. The deposition rates were investigated as a function of sputter pressure, power, gas composition, and substrate temperature. On films deposited over a range of sputter parameters, X-ray diffraction (XRD) and Rutherford backscattering spectrometry (RBS) were performed indicating that optimal deposition conditions for best crystal quality and stoichiometry were a total pressure between 4 and 10 mT, a gas mixture of 85% nitrogen and 15% argon, and a substrate temperature ≈200°C. The films had a weak microcrystalline structure with the *c*-axis preferentially orientated parallel to the substrate normal. MIS capacitors were fabricated on silicon substrates with Ti/Au contacts. Current–voltage (IV) and capacitance–voltage (CV) measurements revealed breakdown fields of 4–12 MV/cm. Depending on the thickness, leakage current densities were between 10^{-10} and 10^{-3} A/cm^2 at 1 V reverse bias, the interface charge density was $\leq 10^{13}$ cm^2, and flat band voltages were from −10 to 2 V. The dielectric permittivity was between 4 and 11 for thick layers (≥100 Å) and decreased to values between 2 and 6 for thicknesses below 100 Å.

PACS: 73.40.Qv (MIS structures)

Keywords: Aluminum nitride; Reactive sputtering; MIS capacitors; Alternative dielectrics

1. Introduction

As the gate oxides of metal–oxide semiconductor field-effect transistors (MOSFETS) shrink to thicknesses below 2 nm, gate leakage currents can become excessive and severely hinder the functionality of the device. Insulators with high dielectric constants are sought as alternatives to silicon dioxide. Compared to low-permittivity gate dielectrics, more channel charge is induced for the same applied gate voltage. Insulators with higher dielectric constants can, therefore, be made thicker, reducing the quantum-mechanical tunneling current. Bulk aluminum nitride (AlN) has a dielectric constant of 9 [1] to 10.4 [2] compared to 3.9 for silicon dioxide, and is thermally stable on silicon, but its behavior in metal–insulator–semiconductor (MIS) devices is still not well understood.

* Corresponding author. Tel.: +1-302-831-8959; fax: +1-302-831-4316.
E-mail address: adam@ee.udel.edu (T. Adam).

0169-4332/01/$ – see front matter
PII: S0169-4332(01)00091-5

Previous studies on reactively sputtered AlN films and their thermal oxides revealed excellent stoichiometries, flat-band voltages, interface state densities [3], and breakdown fields in excess of 0.25 MV/cm [4]. Using reactive radio-frequency (rf) magnetron sputtering, we prepared a series of thick AlN samples over a wide range of deposition conditions. The deposited AlN layers were characterized by X-ray diffraction (XRD), atomic force microscopy (AFM), ellipsometry, and Rutherford backscattering spectrometry (RBS). A series of samples prepared underoptimal deposition conditions with thicknesses between 40 and 600 Å was characterized by capacitance–voltage (CV) and current–voltage (IV) measurements.

2. Experiments

AlN has shown excellent thermal, chemical [5], physical [6], electrical [4], optical [7], and piezoelectrical [8] properties that depend on the deposition method and its specific conditions. It has the widest direct bandgap (6.2 eV) among the III–V materials [1] and has a great potential for optoelectronic devices operating at shorter wavelengths, as well as for high-power and high-temperature devices. Main applications comprise passivation [9], protection [10], encapsulation [11], alternative insulators [12], luminescence [13], buffering gallium nitride growth [14], quantum dot [15] and nanocrystal [16] nucleation, cold cathode emitters [17,18], and effective diffusion barrier caps [19]. Impurities are believed to be responsible for deep states and bandgap reductions [20] and the incorporation of oxygen, carbon, hydrogen, and silicon has been observed in different deposition methods.

2.1. Preparation and deposition

Sputtering was chosen for this study because of its simplicity and low cost. Other techniques such as chemical vapor deposition (CVD) [21], metal organic CVD (MOCVD) [22], laser ablation [23], atomic layer growth [24], vapor pressure epitaxy (VPE) [25], and molecular beam epitaxy (MBE) [26] involve elevated temperatures, expensive reactors, and ultra-high vacuum equipment. Using sputtering, substrate temperatures as low as -172°C [27] and as high as 750°C [28] have yielded stoichiometric AlN with varying crystallographies, but room temperature is generally used. The surface roughness and electrical properties of sputtered AlN films are comparable to epitaxially grown layers, and there is the possibility that amorphous AlN films might experience less leakage due to the absence of the columnar growth, grains, and threading dislocations.

For this study, 3 in. (1 0 0)-oriented p-type silicon wafers of moderate Boron doping levels (1–10 Ω cm) were chemically cleaned to remove surface contaminants and the native oxide, as described elsewhere [29]. Using an Edwards E306A sputter coater with a high-purity Al-target magnetron source, the samples were mounted upside-down to a rotatable water-cooled molybdenum substrate holder 5 cm above two 4 in. targets. The chamber was pumped by a diffusion pump with a liquid nitrogen cold trap to the 10^{-8} T range, typically for a period of 12 h. The partial and total gas pressures were adjusted with mass flow controllers. Prior to deposition, the targets were cleaned by a 10 min medium-power argon plasma at 5 mT with closed shutters.

The sample composition was determined by RBS using 2 MeV helium ions. To characterize the microstructure, the X-ray Θ–2Θ diffraction patterns from $2\Theta = 30$–80° were obtained in a Philips X'Pert MPD system with a fixed stage, Cu Kα radiation, and spatial collimators. The thickness, refractive index, and surface roughness were determined utilizing a 633 nm Rudolph AutoELII ellipsometer with automatic nulling, stylus profilometry, and AFM. Electrical IV and CV measurements were performed on a probe station with coaxial probe tips and an HP4156B and HP4284A, respectively. This setup is capable of measuring static currents in the fA range and capacitances and conductances at frequencies ranging from 20 Hz to 1 MHz.

2.2. Dependence on rf-power

For all considered sputter powers, the thickness of the deposited bulk layers was linearly dependent on sputter time as depicted in Fig. 1a. However, for thicknesses below 200 Å, the growth rate increased by a factor of 2–4 as compared to the bulk rate, indicating a change in sticking coefficient between AlN on silicon and on itself, which needs to be

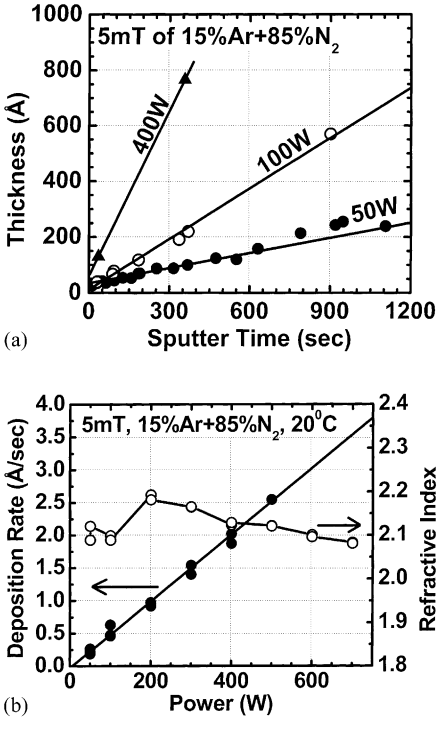

Fig. 1. (a) Aluminum nitride thickness as a function of deposition time and power at room temperature. (b) Deposition rate and refractive index as a function of power for the same gas conditions. The slope of the deposition rate was 0.0051 Å/Ws.

considered for the fabrication of ultra-thin layers. For a 5 mT plasma of 15% argon and 85% nitrogen, the deposition rate of AlN on silicon at room temperature was extracted from the data in Fig. 1 and found to depend linearly on sputtering power with proportional constant of 0.0051 Å/Ws. Weak and broad hexagonal AlN XRD peaks ($\langle 0\,0\,2\rangle$, $\langle 1\,0\,1\rangle$, $\langle 0\,0\,4\rangle$) with relative intensities below 0.5% have been observed for all deposition powers. The films were mostly oriented with their *c*-axis perpendicular to the substrate surface. Higher-powers yielded slightly larger relative X-ray peak intensities. The refractive index was found to be centered around $n = 2.1$, in excellent agreement with published values [30]. Within the detection limits of RBS, the stoichiometry did not depend on rf-power.

2.3. Dependence on gas pressure

The ion mean free path in the region of glow discharge is inversely proportional to the gas density. Therefore, the deposition rate is expected to depend on the gas pressure during sputtering. Using magnetron-type target fixtures, it is possible to achieve a glow discharge over a wide range of pressures. A minimum pressure of 1.5 mT was required to sustain the glow discharge, and pressures over 50 mT resulted in heavy plasma distortions and inhomogeneous layer thicknesses. We prepared a set of samples with a gas mixture of 15% argon and 85% nitrogen at 100 W and varied the deposition pressure between 1.5 and 30 mT. Although, crystallographic phase changes of the deposited AlN layers were observed, XRD peaks showed no significant change in full-width at half-maximum (FWHM) values and relative intensities, while the deposition rate doubled at 1.5 mT and halved at 30 mT, compared to the value at 5 mT. In Fig. 2, the deposition rate is shown as a function of gas pressure. At each pressure, the deposition rate is roughly linearly dependent on the sputtering power. A similar behavior was reported by Joo et al. [30] and Cheng et al. [31] In order to achieve sufficient rate control, capacitance manometers and feedback-controlled gate-valves are recommended for pressure control. Within the detection limit of RBS, no change in stoichiometry with varying total gas pressure was detected.

2.4. Dependence on gas composition

Stoichiometry and impurity levels are expected to influence the band gap states and related electrical

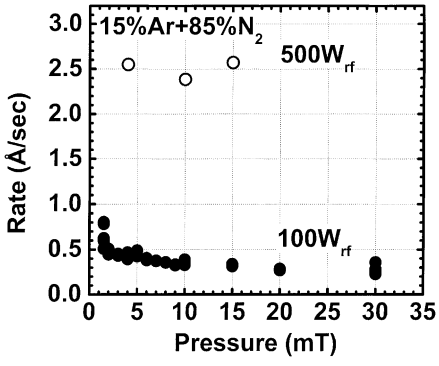

Fig. 2. Sputter deposition rate of aluminum nitride as a function of total gas pressure measured by a pirani-type thermocouple gauge. Varying the gas pressure can change the sputter rate. Compared to 5 mT it has nearly doubled at 1.5 mT, the lowest possible discharge pressure.

properties. For example, if the dielectric AlN layer is aluminum rich, dangling Al bonds are believed to give rise to 1 eV deep states [32]. As reported by Fara et al. [33], nitrogen vacancies occur as states in the bandgap 2–2.5 eV above the valence band. Incorporated oxygen is reported to yield states 0.5–1.9 eV above the valence band, while silicon and carbon yield states 0.9 and 1.2 eV below the conduction band, respectively. Most groups experienced difficulties with the incorporation of oxygen and carbon. The resulting states may pin the Fermi level, which has been observed in capacitance-voltage sweeps [4,9,12]. They have been classified as fast states due to the appearance of kinks and stretching in 1 MHz CV curves.

We prepared a series of samples with layers of AlN having a thickness of 2000 Å and varied the concentration of argon in the argon–nitrogen gas mix. The total gas pressure was held constant at 5 mT and the layers were sputtered at 400 W and room temperature. RBS revealed that the resulting layer compositions were $Al_{50\%}N_{50\%}$ for almost the entire concentration range. Only for extremely high argon concentrations did we find slightly aluminum rich layers, and both the deposition rate and refractive index increased considerably. For layers deposited in pure nitrogen (0% Ar), hexagonal AlN XRD peaks were still visible in the XRD sweeps, but RBS showed considerable oxygen incorporation. At higher argon concentrations, weak XRD peaks from different orientations became visible, as also reported by Cheng et al. [31]. A pure argon gas resulted in the deposition of aluminum. As shown in Fig. 3, the deposition rate and refractive index were found to be reasonably constant between 0 and 60% of argon.

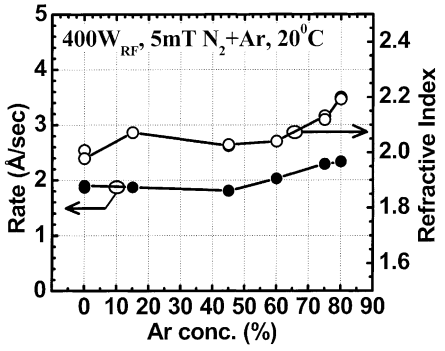

Fig. 3. Dependence of deposition rate and refractive index on the argon concentration in the reactive gas. A pure argon gas (100% Ar) yielded in the deposition of aluminum.

2.5. Substrate temperature

Similar to MBE, CVD, laser ablation, and VPE, the raised substrate temperatures are expected to increase the ad-atom mobility during sputtering, although, the kinetics of the arriving species is different. To study the effect of the substrate temperature, samples were attached to a boron nitride coated graphite heater element by a quartz-glass enclosed titanium-wire spring. The heater element was placed inside a

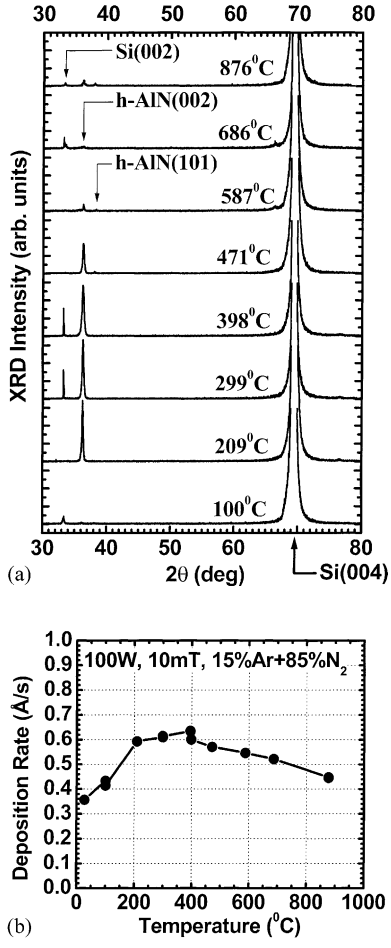

Fig. 4. (a) Cu Kα XRD spectra of samples deposited at different substrate temperatures for times between 95 and 115 min with a power of 100 W and 10 mT of 15% Ar and 85% N_2. (b) Deposition rate measured by ellipsometry.

water-cooled stainless steel cell, and the temperature was measured at the backside of the heater element by a thermocouple. All samples were sputtered at 100 W in 10 mT of 15% argon and 85% nitrogen for durations between 95 and 115 min. As indicated in Fig. 4(a), the (0 0 2) AlN diffraction peak was strongest in the range of 200–500°C, where its FWHM and relative intensity value reached $\Delta\Theta = 0.04°$ and 27%, respectively. The deposition rate in Fig. 4(b) showed a maximum at temperatures between 200 and 500°C.

2.6. Electrical characterization

We prepared a series of MIS capacitors with AlN insulators sputtered at room-temperature using powers of 50 and 100 W with 5 mT of 15% argon and 85% nitrogen. High temperature nitrogen and oxygen treatments were performed in a horizontal open-end quartz-glass tube furnace. The samples were slowly inserted (3 inch/min), annealed in N_2 or oxidized in dry O_2 at 750 or 800°C, and removed with 3 inch/min. Samples with thicknesses larger than 300 Å tended to form visible defects. Therefore, we fabricated AlN layers on p-type (1 0 0) Si with thicknesses below 300 Å in addition to one reference sample with 570 Å. After the deposition and high-temperature steps, 150 Å of high-purity titanium was e-beam evaporated to protect the AlN layer from contamination and subsequent photolithography steps. As reported by Mileham et al. [5], KOH-based developer etches AlN at a very fast rate. Exposing AlN to RD6 developer etched 4000 Å in 10 min. We patterned circular dots with an area of 3.621×10^{-5} cm^2 using lift-off with Ti:Au (100 Å:5 kÅ). Before developing, the backside of the silicon substrate was made hydrophobic by immersing the samples in buffer oxide etch (1:10) for 30 s. The backside (150 Å:2 kÅ of Ti:Au) was metallized without breaking vacuum by rotating the sample holder. After lift-off, the dots were

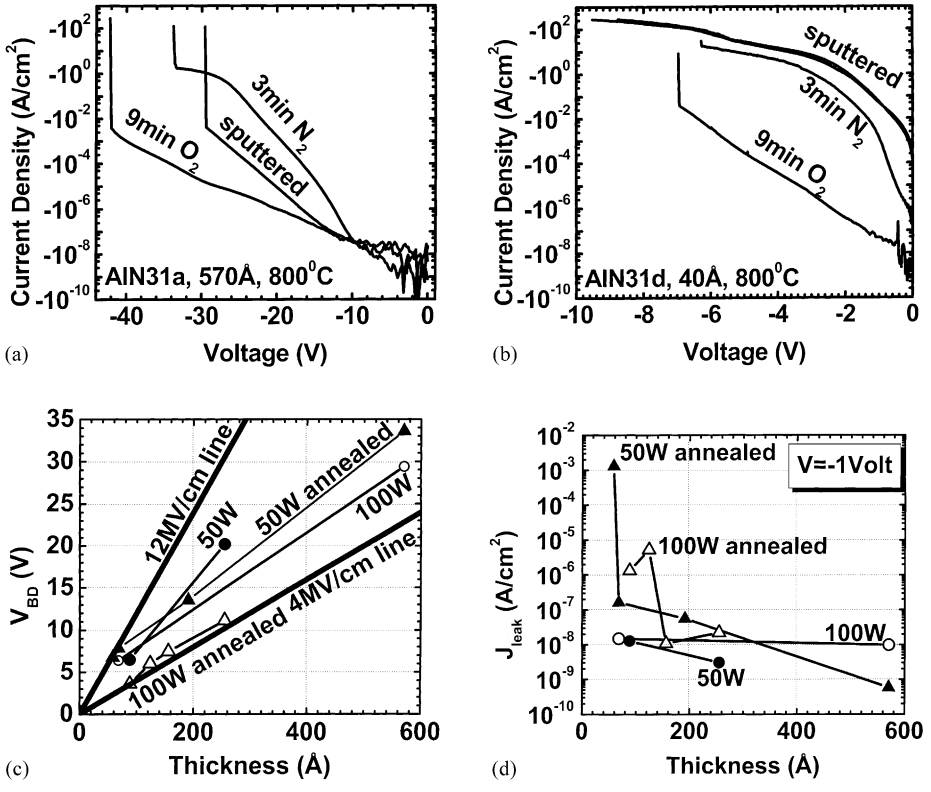

Fig. 5. Top: current density vs. voltage sweeps of the thickest (left) and thinnest (right) sample. Bottom: breakdown voltage vs. thickness (left) and leakage current density versus thickness (right), extracted at 1 V reverse bias. Thermally grown SiO_2 has breakdown strengths of 10 MV/cm [1].

electrically isolated by a short reactive ion etch using an SF_6-based chemistry.

CV and IV measurements showed hysteresis and initial negative differential resistivity (NDR) bumps between forward and reverse sweeps, indicating mobile charges trapped inside the AlN. Before performing the IV measurements, the samples were swept well below breakdown until the NDR disappeared, and held at zero volts until the current had settled. Each point was allowed settling for 20 s and then measured by averaging over a period of 1.6 s. All samples were measured through breakdown and then re-measured after failure. As indicated in Fig. 5, most of the as-sputtered samples showed considerable leakage, which could be reduced by orders of magnitude by annealing in nitrogen. A further reduction in leakage current and an increase in breakdown voltage were achieved by annealing in oxygen. However, sputtered AlN has been shown to form Al_2O_3 under high-temperature oxygen treatments with an increase in thickness by a factor of 1.3–1.7 [3]. As shown in Fig. 5c, we measured breakdown fields between 4 and 12 MV/cm ($E_{BD}^{SiO_2} = 10\,MV/cm$) [1] and leakage current densities below 10^{-6} A/cm^2, extracted at –1 V, although, larger leakage currents occur at increased biases. The currents of as-sputtered and annealed AlN could not be fitted to either Fowler–Nordheim tunneling or Frenkel–Poole emission transport mechanisms.

To avoid hysteresis, separate capacitance voltage curves were taken from zero to depletion and from zero to accumulation. All samples were biased below breakdown at gradually reducing positive and negative dc voltages. Subsequently, a zero bias was applied to the device under test for 1 min before sweeping to depletion. The same cycling procedure was repeated before measuring the accumulation region, which resulted in negligible discontinuities in C at 0 V. Fig. 6 shows representative CV sweeps of the

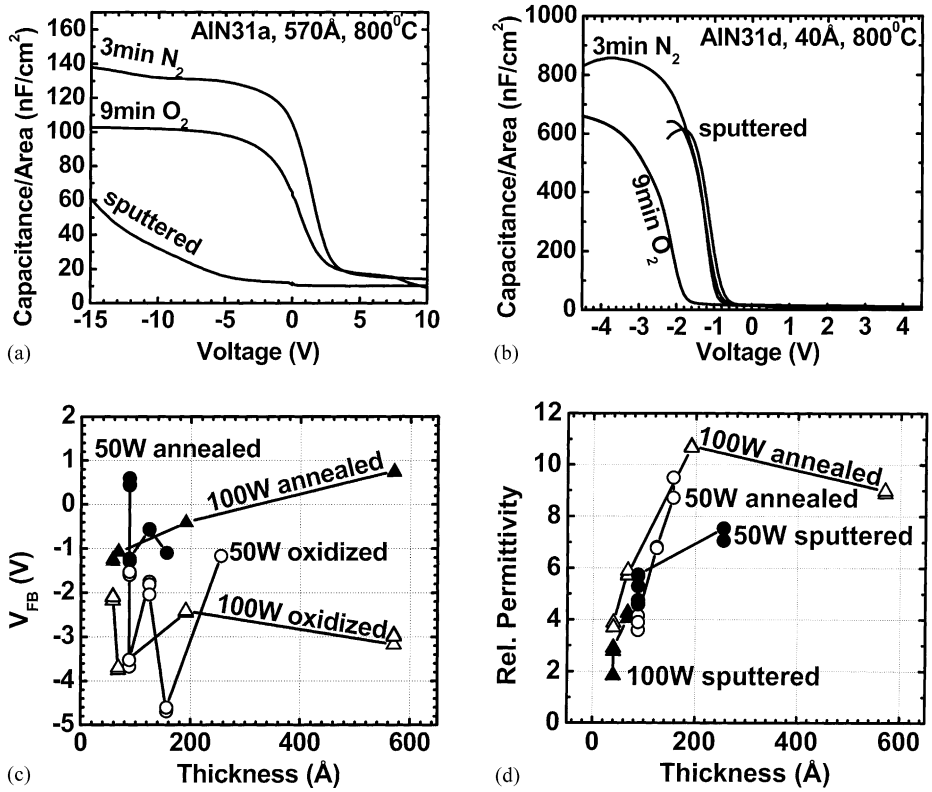

Fig. 6. Top: capacitance per area vs. voltage curves for the thickest (left) and thinnest (right) sample. Bottom: flat band voltage (left) and relative permittivity (right) vs. AlN layer thickness. The relative dielectric constant was extracted from the maximum measurable capacitances.

570 Å reference sample and the thinnest sample (40 Å). Similar to MOS capacitors with SiO_2, our capacitors showed accumulation and depletion, although, inversion could not be achieved at medium and low frequencies. We suspect a large number of fast recombination centers at the interface that efficiently capture minority carriers. In addition, for most of the as-sputtered samples, we observed a strong stretching of the CV curves. Annealing in nitrogen and oxygen at 750 and 800°C proved to reduce the stretching. However, the remaining stretch-out did not allow fitting to theory in both the accumulation and depletion region. Furthermore, low breakdown voltages and large leakage currents at higher accumulation biases severely interfered with the measurement of the capacitance. The measured flat band voltages are indicative of a large density of integrated interface states ($<10^{13}$ cm^2). The relative permittivity calculated from the maximum capacitances was 4 to 11 for samples having a layer thickness above 100 Å and 2–6 for layers below 100 Å. Compared to thermally grown silicon dioxide ($\varepsilon = 3.9$), this increase in permittivity would permit a 200 Å AlN layer to replace SiO_2 as thin as 71 Å, provided that leakage currents and flat band voltages can be reduced.

3. Conclusions

We have investigated a wide range of deposition conditions for the reactive radio-frequency magnetron sputtering of AlN on 1–10 Ω cm p-type (1 0 0) silicon substrates. The quality (stoichiometry, crystallography, refractive index) and deposition rate were presented as a function of gas pressure, gas composition, sputtering power, and substrate temperature. Optimal conditions for the best *c*-axis oriented crystal quality at 100 W were identified to be a gas pressure of 10 mT, a gas composition of 15% argon and 85% nitrogen, and a substrate temperature around 200°C, where the deposition rate approached a maximum. Thin layers of as-sputtered AlN revealed large leakage currents and flat band voltages, which were mitigated by annealing in nitrogen or oxygen. Breakdown fields were between 4 and 12 MV/cm and dielectric permittivities between 2 and 11 making sputtered AlN an attractive low-temperature low-cost alternative dielectric material to thermally oxidized silicon. However, the inability to create minority carriers at the semiconductor surface, probably due to a large density of fast recombination centers at the insulator–semiconductor interface, indicates that more work is necessary before the integration into MOS transistor circuits becomes feasible.

Acknowledgements

We gratefully acknowledge the support from the Intel Corporation and the National Science Foundation (SGER grant number ECS-9872692). Special thanks to G. Bai and L. Manchanda for helpful discussions.

References

[1] Ottfried Madelung (Ed.), Semiconductors — Basic Data, Springer, Heidelberg, 1996.
[2] M.-A. Dubois, P. Mulalt, Properties of aluminum nitride thin films for piezoelectric transducers and microwave filter applications, Appl. Phys. Lett. 74 (20) (1999) 3032.
[3] J. Kolodzey, E.A. Chowdhury, G. Qui, J. Olowolafe, C.P. Swann, K.M. Unruh, J. Suehle, R.G. Wilson, J.M. Zavada, The effects of oxidation temperature on the capacitance–voltage characteristics of oxidized AlN films on silicon, Appl. Phys. Lett. 71 (26) (1997) 3802.
[4] K.S. Stevens, M. Kinniburgh, A.F. Schwartzmann, A. Ohtani, R. Beresford, Demonstration of a silicon field-effect transistor using AlN as the gate dielectric, Appl. Phys. Lett. 66 (23) (1995) 3179.
[5] J.R. Mileham, S.J. Pearton, C.R. Abernathy, J.D. MacKenzie, R.J. Shul, S.P. Kilcoyne, Patterning of AlN, InN, and GaN in KOH-based solutions, J. Vac. Sci. Technol. A 14 (3) (1996) 836.
[6] Yoshihisa Watanabe, Shingo Uchiyama, Yoshikazu Nakamura, Chunlang Li, Tohru Sekino, Koichi Niihara, Mechanical properties and residual stress in AlN/Al mixed films prepared by ion-beam-assisted deposition, J. Vac. Sci. Technol. A 17 (2) (1999) 603.
[7] G.T. Kiehne, G.K.L. Wong, J.B. Ketterson, Optical second-harmonic generation in sputter-deposited AlN films, J. Appl. Phys. 84 (11) (1998) 5922.
[8] D. Liufu, K.C. Kao, Piezoelectric, dielectric, and interfacial properties of aluminum nitride films, J. Vac. Sci. Technol. A 16 (4) (1998) 2360.
[9] C.-M. Zetterling, M. Östling, K. Wongchotigul, M.G. Spencer, X. Tang, C.I. Harris, N. Nordell, S.S. Wong, Investigation of aluminum nitride grown by metal–organic chemical–vapor deposition on silicon carbide, J. Appl. Phys. 82 (6) (1997) 2990.
[10] X.S. Miao, Y.C. Chan, E.Y.B. Pun, A new protective AlN film for organic photoconductors, Appl. Phys. Lett. 71 (2) (1997) 184.

[11] K.A. Jones, K. Xie, D.W. Eckart, M.C. Wood, V. Talyansky, R.D. Vispute, T. Venkatesan, K. Wongchotigul, M. Spencer, AlN as an encapsulate for annealing SiC, J. Appl. Phys. 83 (12) (1998) 8010.
[12] C.-M. Zetterling, M. Östling, N. Nordell, O. Schön, M. Deschler, Influence of growth conditions on electrical characteristics of AlN on SiC, Appl. Phys. Lett. 70 (24) (1997) 3549.
[13] W.M. Jadwisienczak, H.J. Lozykowski, F. Perjeru, H. Chen, M. Kordesch, I.G. Brown, Luminescence of Tb ions implanted into amorphous AlN thin films grown by sputtering, Appl. Phys. Lett. 76 (23) (2000) 3376.
[14] P. Waltereit, O. Brandt, A. Trampert, M. Ramsteiner, M. Reiche, M. Qi, K.H. Ploog, Influence of AlN nucleation layers on growth mode and strain relief of GaN on 6H-SiC(0 0 0 1), Appl. Phys. Lett. 74 (24) (1999) 3660.
[15] J.L. Rouvière, J. Simon, N. Pelekanos, B. Daudin, G. Feuillet, Preferential nucleation of GaN quantum dots at the edge of AlN threading dislocations, Appl. Phys. Lett. 75 (17) (1999) 2632.
[16] K.M. Hassan, A.K. Sharma, J. Narayan, J.F. Muth, C.W. Teng, R.M. Kolbas, Optical and structural studies of Ge nanocrystals embedded in AlN matrix fabricated by pulsed laser deposition, Appl. Phys. Lett. 75 (9) (1999) 1222.
[17] A.T. Sowers, J.A. Christman, M.D. Bremser, B.L. Ward, R.F. Davis, R.J. Nemanich, Thin films of aluminum nitride and aluminum gallium nitride for cold cathode applications, Appl. Phys. Lett. 71 (16) (1997) 2289.
[18] C.I. Wu, A. Kahn, Negative electron affinity at the Cs/AlN(0 0 0 1) surface, Appl. Phys. Lett. 74 (10) (1999) 1433.
[19] Evan M. Handy, Mulpuri V. Rao, K.A. Jones, M.A. Derenge, P.H. Chi, R.D. Vispute, T. Venkatesan, N.A. Papanicolaou, J. Mittereder, Effectiveness of AlN encapsulant in annealing ion-implated SiC, J. Appl. Phys. 86 (2) (1999) 746.
[20] M. Katsikini, E.C. Paloura, T.S. Cheng, C.T. Foxon, Determination of the local microstructrure of epitaxial AlN by X-ray absorption, J. Appl. Phys. 82 (3) (1997) 1166.
[21] I.L. Guy, S. Muensit, E.M. Goldys, Extensional piezoelectric coefficients of gallium nitride and aluminum nitride, Appl. Phys. Lett. 75 (26) (1999) 4133.
[22] K. Dovidenko, S. Oktyabrsky, J. Narayan, Characteristics of stacking faults in AlN thin films, J. Appl. Phys. 82 (9) (1997) 4296.
[23] Y.F. Lu, Z.M. Ren, T.C. Chong, B.A. Cheong, S.K. Chow, J.P. Wang, Ion-assisted pulsed laser deposition of aluminum nitride thin films, J. Appl. Phys. 87 (3) (2000) 1540.
[24] Herng Liu, J.W. Rogers Jr., Molecularly engineered low temperature atomic layer growth of aluminum nitride on Si(1 0 0), J. Vac. Sci. Technol. A 17 (2) (1999) 325.
[25] L.J. Schowalter, Y. Shusterman, R. Wang, I. Bhat, G. Arunmozhi, G.A. Slack, Epitaxial growth of AlN and $Al_{0.5}Ga_{0.5}N$ layers on aluminum nitride substrates, Appl. Phys. Lett. 76 (8) (2000) 985.
[26] Z.Y. Fan, G. Rong, N. Newman, J. Smith, Defect annihilation in AlN thin films by ultrahigh temperature processing, Appl. Phys. Lett. 76 (14) (2000) 1839.
[27] K. Gurumurugan, H. Chen, G.R. Harp, W.M. Jadwisienczak, H.J. Lozykowski, Visible cathodoluminescence of Er-doped amorphous AlN thin films, Appl. Phys. Lett. 74 (20) (1999) 3008.
[28] K. Jagannadham, A.K. Sharma, Q. Wei, R. Kalyanraman, J. Narayan, Structural characteristics of AlN films deposited by pulsed laser deposition and reactive magnetron sputtering: a comparative study, J. Vac. Sci. Technol. A 16 (5) (1998) 2804.
[29] B.A. Orner, Growth and optical study of group IV semiconductor alloys and group IV heterostructure devices, Dissertation, University of Delaware, Newark, DE 19716, May 1997.
[30] Han-Yong Joo, Hyeong Joon Kim, Sang June Kim, Sang Youl Kim, Spectrophotometric analysis of aluminum nitride thin films, J. Vac. Sci. Technol. A 17 (3) (1999) 862.
[31] Chien-Chuan Cheng, Ying-Chung Chen, Horng-Jwo Wang, Wen-Rong Chen, Low-temperature growth of aluminum nitride thin films on silicon by reactive radio frequency magnetron sputtering, J. Vac. Sci. Technol. A 14 (4) (1996) 2238.
[32] C.I. Wu, A. Kahn, Electronic states at the aluminum nitride(0 0 0 1)-1 × 1 surfaces, Appl. Phys. Lett. 74 (4) (1999) 546.
[33] Antonella Fara, Fabio Bernardini, Vincenzo Fiorentini, Theoretical evidence for the semi-insulating character of AlN, J. Appl. Phys. 85 (3) (1999) 2001.